Modeling the Size and Shape of Saturn's Magnetopause with Variable Dynamic Pressure

C.S. Arridge, N. Achilleos, and M.K. Dougherty

Space and Atmospheric Physics Group, Imperial College London, UK

K.K. Khurana and C.T. Russell

Institute of Geophysics and Planetary Physics, UCLA, USA

Abstract.

The location and shape of a planetary magnetopause is principally determined by the dynamic pressure, D_p, of the solar wind, the orientation of the planet's magnetic dipole with respect to the solar wind flow, and by the distribution of stresses inside the magnetosphere. The magnetospheres of Saturn and Jupiter have strong internal plasma sources compared to the solar wind source and also rotate rapidly, causing an equatorial inflation of the magnetosphere and consequently the magnetopause. Empirical studies using Voyager and Pioneer data concluded that the kronian magnetopause was Earth-like in terms of its dynamics [*Slavin et al.*, 1985] as revealed by how the position of the magnetopause varies with dynamic pressure.

In this paper we present a new pressure-dependent model of Saturn's magnetopause, using the functional form proposed by *Shue et al.* [1997]. To establish the pressure-dependence we also use a new technique for fitting a pressure-dependent model in the absence of simultaneous upstream pressure measurements. Using a Newtonian form of the pressure balance across the magnetopause boundary, and using model rather than minimum variance normals, we estimate the solar wind dynamic pressure at each crossing. By iteratively fitting our model to magnetopause crossings observed by the Cassini and Voyager spacecraft, in parallel with the pressure balance, we obtain a model which is self-consistent with the dynamic pressure estimates obtained. We find a model whose size varies as $\sim D_p^{-1/4.6}$ and whose flaring decreases with increasing dynamic pressure. This is interpreted in terms of a different distribution of fields and particles stresses which has more in common with the jovian magnetosphere compared with the terrestrial situation. We also make first-order corrections to account for the tilt between the planetary dipole and the solar-wind flow.

We compare our model with the existing models of the magnetopause and highlight the very different geometries. We find our results are consistent with recent MHD modeling of Saturn's magnetosphere [*Hansen et al.*, 2005]. The effect of our magnetopause model on the bow shock is also studied, in particular how changes in dynamic pressure affect the stand-off position of the shock. It is found that as the dynamic pressure increases the shock can approach the magnetopause more closely, responding to the more streamlined shape of our model at higher pressures.

1. Introduction

The magnetopause is a highly structured boundary formed by the interaction between the shocked sub-magnetosonic solar wind and the essentially dipolar field of a magnetized body [e.g. *Russell*, 2003]. The equilibrium magnetopause has a complex three-dimensional geometry, and forty years after the discovery of the terrestrial magnetopause a general understanding of the size and global shape of planetary magnetopauses is still a topic of intense research [e.g. *Kawano et al.*, 1999; *Shue et al.*, 1997, 2000; *Shue and Song*, 2002].

The location of the terrestrial magnetopause is determined principally by the strength and orientation of both the planetary magnetic dipole and interplanetary mag-

0148-0227/06/$9.00

netic field (IMF) (particularly the IMF component projected onto the planetary magnetic dipole). In contrast to the size, the shape of a planetary magnetopause is crucially determined by the distribution of stress inside the magnetosphere. Spacecraft missions to the outer planets have revealed rapidly rotating magnetospheres with strong internal sources of plasma, leading to an equatorial inflation of their magnetospheres and corresponding magnetopause boundaries. Hence, the size and shape of the outer planet magnetopause boundaries are also a function of plasma content and planetary rotation rate. This equatorial inflation is revealed by a polar flattening of the magnetopause and has been observed in theoretical [*Joy et al.*, 2002] and empirical [*Huddleston et al.*, 1998] models of the jovian boundary. The effect of the stress distribution is also revealed by how the magnetopause responds to the solar wind. A similar effect is expected at Saturn because of its rapid rotation and the presence of plasma from the rings, ionosphere and icy moons [*Blanc et al.*, 2002].

The pressure-dependent size of the terrestrial magnetopause can be calculated from the interaction of a flowing plasma with a vacuum dipole field. This simple analysis yields a magnetopause size that varies with the $-1/6$ power of the dynamic pressure, and which has been confirmed in empirical models of the terrestrial magnetopause [e.g. *Shue et al.*, 1997]. A further interesting observation in these models is that the flaring of the tail increases with increasing dynamic pressure. This is understood in terms of reconnection adding magnetic flux into the tail and increasing its size.

The organization of internal plasma sources into a magnetodisc in the jovian magnetosphere has two observable effects on these aspects, compared to the case of the Earth. The first is that the presence of plasma breaks the vacuum dipole assumption in calculating the size of the magnetopause, increasing the power law exponent to between $-1/4$ and $-1/5$ [*Huddleston et al.*, 1998]. The second is that the tail flaring decreases with increasing dynamic pressure, in stark contrast to the terrestrial situation. The magnetic pressure of the dipole field balances the dynamic pressure in the terrestrial case, but at Jupiter the hot plasma pressure and centrifugal force on the cold plasma are as important as the magnetic pressure in determining the shape of the magnetopause. *Huddleston et al.* [1998] interpreted their observations in terms of these additional sources of stress. At low dynamic pressures the hot plasma pressure can balloon the magnetic field and increase the magnetopause flaring, whereas at high dynamic pressures the centrifugal force forces the magnetopause into a more disc-like shape and the flaring decreases. Given internal mass loading and rapid rotation of Saturn's magnetosphere we might expect a similar effect on Saturn's magnetopause. The limited spatial exploration of outer planet magnetopauses, coupled with the relative absence of consistent upstream monitors means that the role of mass loading and rotation in determining the magnetopause shape at the outer planets has not been fully explored in a time-dependent fashion.

1.1. Previous Models of Saturn's Magnetopause

The only empirical model of Saturn's magnetopause [*Slavin et al.*, 1983, 1985] was developed by fitting a three-parameter second order conic section to a subset of magnetopause crossings, identified in Pioneer 11 and Voyager 1/2 plasma and magnetometer data. *Slavin et al.* [1983, 1985] were primarily interested in the behavior of the dayside magnetopause, so the outbound Voyager 1

crossings were not included in their fitting. The presence of boundary waves or other oscillations were taken into account by averaging together crossings that occurred within 10 hours of each other. The final set of crossings (in an unaberrated coordinate system) were fitted to the model using least squares fit where the deviations normal to the model surface were minimized [*Slavin and Holzer*, 1981].

To reduce the scatter in the fit the crossings were pressure corrected and the model re-fitted. This was carried out by determining the dynamic pressure, D_p, at each crossing using the observed field just inside the magnetopause, the flaring angle, Ψ, as estimated from a minimum variance analysis of the magnetometer data [*Sonnerup and Cahill*, 1967], and a Newtonian pressure balance [*Spreiter and Alksne*, 1970]. The stand-off (distance between the planet and the subsolar point on the magnetopause) distance for each crossing was determined using the magnetopause shape model from the initial fit. The corresponding stand-off distances and pressures were combined to estimate the power-law behavior of the stand-off distance, $r_0 \sim D_p^{-\alpha}$, which was then used to pressure-correct the crossings and hence the model fit. Their model exhibits a power-law scaling of the magnetopause size versus dynamic pressure $r_0 = 10.04 D_p^{-1/6.1}$, i.e., a terrestrial-type size behavior, where D_p is in nanoPascals and r_0 is in planetary radii ($1R_S = 60268km$).

Three theoretical studies have focused on the shape of Saturn's magnetopause. *Stahara et al.* [1989] developed a gas-dynamic model which showed that the polar flattening of the magnetopause was intermediate between the Earth and Jupiter. *Macek et al.* [1992] mainly concentrated on the geometry of the distant tail. By numerically solving equations conserving energy and plasma density, magnetic field, and momentum at the tail magnetopause, they showed that Saturn's magnetotail radius rapidly approached $\approx 80R_S$ at a down-tail distance of $\approx 100R_S$. Closer to the planet at around $50R_S$ tailward, the calculated tail radius was approximately $50R_S$. They also showed that the tail was strongly flattened in the z direction even at moderately close distances ($200R_S$) indicating a strong polar flattening. Unless explicitly stated, we will work in solar magnetospheric (SM) coordinates where $\hat{\mathbf{x}}$ is directed towards the sun, $\hat{\mathbf{y}} = \hat{\mathbf{M}} \times \hat{\mathbf{x}}$ and $\hat{\mathbf{z}}$ completes the right-handed set where the $X - Z$ plane contains the planetary magnetic dipole. Thus solar magnetospheric coordinates at Saturn are termed KSM, and are directly equivalent to terrestrial GSM and jovian JSM.

The most comprehensive theoretical model of Saturn's magnetopause was developed by *Maurice et al.* [1996] (MEBS). This was a by-product of their global model of Saturn's magnetospheric magnetic field, developed using the self-consistent methods of *Mead and Beard* [1964]. By iteratively evaluating the force balance between the ring current and dipole magnetic fields in the magnetosphere, and the dynamic pressure of the solar wind, the method simultaneously solves for both the Chapman-Ferraro currents and the size and shape of the magnetopause. The resulting surface was fitted to a conic section, written in a cartesian form (1) with 10 free parameters in two polynomials, g and h. It describes ellipses in the $Y - Z$ plane to allow the model to describe polar flattening, and in the $X - Z$ plane the model is general enough to resolve the cusp.

$$1 = \frac{y^2}{h(x)} + \frac{z^2}{g(x)} \tag{1}$$

Where $g(x)$ and $h(x)$ are defined by (2), $\{x_c, 0, \sqrt{g(x_c)}\}$ are the coordinates of the cusp, and x_t is a down-tail distance where the MP stops flaring. Their fitting was carried out, by least squares, for different stand-off distances, giving a model geometry that is a function of the stand-off distance, r_0, unlike the self-similar Slavin model, and hence the coefficients in (2) are functions of r_0.

$$g(x) = (a_0 + a_1 x)(r_0 - x) \qquad x_c \leq x < r_0 \tag{2a}$$

$$g(x) = (b_0 + b_1 x + b_2 x^2)(x_c - x) + z_c^2 \qquad -100 \leq x < x_c \tag{2b}$$

$$h(x) = (c_0 + c_1 x + c_2 x^2)(r_0 - x) \qquad x_t \leq x < r_0 \tag{2c}$$

$$h(x) = (c_0 + c_1 x_t + c_2 x_t^2)(r_0 - x_t) \qquad x > x_t \tag{2d}$$

Whilst not being too dissimilar at the nose, the geometry of Slavin versus MEBS at the flanks is quite different. The hyperbolic Slavin model flares asymptotically whereas the MEBS shape has an elliptic tail cross-section with a constant tail radius of $\approx 40 R_S$ in the $X-Y$ plane. The empirical Slavin model ignored asymmetries introduced by the tilt of the dipole to the solar-wind flow but this was of no concern since the model was developed on crossings near Saturn's equinox. MEBS has some dipole tilt dependence but is limited to certain tilt angles beyond which interpolation between coefficients must be applied. Furthermore only the change in geometry with stand-off distance was studied in the MEBS model, so no connection to the solar wind dynamic pressure was established.

1.2. This Study

A persistent problem for outer planetary magnetosphere research is the lack of dynamic pressure measurements, or more properly, the lack of a consistent upstream solar wind monitor. This limits how much can be done in studying the magnetopause or internal magnetospheric dynamics. For a study of the magnetopause shape, it makes it very difficult to develop pressure-dependent models of this boundary.

In this paper we present a new technique for building pressure-dependent magnetopause models and apply this method to a dataset of magnetopause crossings from Voyager and Cassini. We use a relatively new functional form [*Shue et al.*, 1997] to describe the magnetopause which is quite flexible and not only allows the size to be pressure-dependent, but also the shape - particularly the degree to which the magnetotail is flared.

In the following section we present our technique for obtaining dynamic pressure estimates in the absence of an upstream monitor and demonstrate our technique for building a pressure-dependent model. In section 3 we discuss the dataset and how these data were obtained and processed. Our method is applied to the data in section 4 and we discuss the stability and physical implications of our model. We also compare our new model to the *Slavin et al.* [1983, 1985] and *Mead and Beard* [1964] models using the same dataset.

2. Methods

2.1. Estimating the Dynamic Pressure

A typical approach [e.g. *Slavin et al.*, 1983] for estimat-

ing the upstream dynamic pressure at a magnetopause crossing observed by a spacecraft, is to reconstruct the pressure balance, which is assumed to be holding the boundary in dynamical equilibrium. Assuming such an equilibrium exists and using a Newtonian pressure balance [*Spreiter and Alksne*, 1970], the magnetic pressure just inside the magnetopause is holding off the dynamic pressure of the solar wind, viz. $B_{MS}^2/2\mu_0 = kD_p \cos^2\Psi$ where B_{MS} is the magnetospheric magnetic field just inside the magnetopause, k is a factor of the order unity, and Ψ is the angle between the solar wind direction (assumed to be along $-\hat{\mathbf{x}}$) and the local normal to the magnetopause (the flaring angle). The canonical approach is to measure B_{MS} from magnetometer data, and to estimate Ψ by subjecting magnetometer data to a minimum variance analysis [*Sonnerup and Cahill*, 1967]. The value of D_p can then be calculated using these quantities in the pressure balance equation.

Several issues are evident at this point. As discussed in the introduction, the plasma stresses in outer planet magnetospheres are comparable to the magnetic pressure. It follows that by only including the magnetic pressure in this pressure balance we are underestimating the dynamic pressure, perhaps by up to a factor of two. Secondly the assumption of pressure balance implicitly assumes the magnetopause is static. Such an equilibrium is almost certainly never observed and leads to a bias between sheath-magnetosphere and magnetosphere-sheath pressure estimates. When the spacecraft emerges from the magnetosphere into the magnetosheath the dynamic pressure is 'winning'in the pressure balance, and any dynamic pressure estimates that are made will necessarily be too low since the magnetopause is moving inwards. A vice-versa argument can be made for estimates made when the spacecraft moves into the magnetosphere. Possible effects of these issues will be discussed at the end of this paper.

We use a variant of this pressure balance technique in order to estimate the dynamic pressure. In the absence of flaring angles from minimum variance analysis, we obtain Ψ directly from a model of the magnetopause, suitably scaled to match the magnetopause crossing in question. So, given a crossing, the model is scaled so that it passes through the spacecraft position. The normal vector to the model surface is calculated at the position of the spacecraft and the flaring angle calculated from the scalar product of the model normal with the solar wind direction. Of course this makes the angle Ψ model-dependent. The rationale for this approach is that in the assumed equilibrium the magnetopause geometry affects the pressure balance and thus the dynamic pressure is inferred based on this assumption.

A more elaborate form of the pressure balance is also used. As the flaring angle decreases, it is expected that the role of solar wind (or magnetosheath) thermal pressure becomes increasingly important because of the $\cos^2\Psi$ factor in determining the pressure balance – in effect compressing the tail to a greater degree than would occur in the absence of thermal pressure. To attempt to take this into account we use a form of the pressure balance which incorporates the pressure balance between the solar wind thermal (static) and dynamic pressures, and the magnetospheric magnetic field. Equation (3) expresses this pressure balance. The introduction of the $\sin^2\Psi$ dependence satisfies the demands of hydrodynamic flow far down-tail and near the stagnation streamline [*Petrinec and Russell*, 1997].

The value of k is used to extrapolate from a measurement in the sheath, to the solar-wind value and is a factor

close to unity as previously described. We set $k = 0.881$ which is valid in high Mach number régime [*Spreiter and Alksne*, 1970] such as observed at Saturn (Achilleos et al., submitted).

$$\frac{B_{MS}^2}{2\mu_0} = kD_p \cos^2\Psi + P_0 \sin^2\Psi \tag{3}$$

The static pressure in the solar wind is assigned a fixed value of $10^{-4} nPa$ derived from average solar wind values [*Slavin et al.*, 1985]. Obviously near the nose of the magnetopause the dynamic pressure term dominates, but at larger distances in the downstream direction the static pressure becomes comparable to, and eventually dominates over the dynamic pressure.

This form of the pressure balance is used to fit our new model and also to examine the models of *Slavin et al.* [1983, 1985] and *Maurice et al.* [1996] in section 4.3.

2.2. Modeling the Magnetopause

In fitting a model magnetopause shape with pressure-dependence we require dynamic pressure values for each magnetopause crossing but as we have pointed out, such simultaneous measurements are not available at Saturn. Our method consists of iteratively fitting the magnetopause shape, and at each iteration of the solver applying the method described in the previous section to estimate the dynamic pressure at each crossing, using the currently fitted model to obtain Ψ at each crossing. Thus as the non-linear fitting routine adjusts the parameters of the shape model, the model normals and hence the dynamic pressure estimates also change. The solver iterates until the RMS residual and the parameters of the model reach a tolerance of 10^{-6}.

We have applied this method using the functional form described by *Shue et al.* [1997] which has been used to model the terrestrial magnetopause. This functional form (4) is particularly flexible in that it allows a boundary which is either closed or open depending on the value of the exponent, K. For $K > 0.5$ the magnetopause is open, and for $K < 0.5$ the magnetopause is closed. See figure 1 in *Shue et al.* [1997] for an illustration of the behavior of this form for different values of K (called α in their paper). The constant factor r_0 represents the stand-off distance of the magnetopause at the subsolar point.

$$r = r_0 \left(\frac{2}{1 + \cos\theta} \right)^K \tag{4}$$

Here (r, θ) are the polar coordinates of a point on the magnetopause, axially symmetric about the x axis, θ is the angle from the x axis to the point and r is the distance from the planet to the point. In the canonical terrestrial approach, r_0 and K are functions of D_p and IMF orientation and a fitting is carried out using upstream observations coinciding with the observed magnetopause crossings. *Shue et al.* [1997] made r_0 and K a function of D_p and IMF B_z. The role of the IMF orientation in controlling Saturn's magnetospheric dynamics is unclear [*Crary et al.*, 2005] and accurate determinations of the IMF orientation may be difficult to extract from magnetosheath data so we restrict our attention to pressure dependence, neglecting the IMF. We make r_0 and K a function of D_p alone by adapting the forms used in *Shue et al.* [1997] (see their equations 10 and 11):

$$r_0 = a_1 D_p^{-a_2} \tag{5a}$$

$$K = a_3 + a_4 D_p \tag{5b}$$

By substituting these forms into (4) we use our method to fit for the coefficients a_i. We use a non-linear fitting routine, based on an interior-reflective Newton method to find the a_i's by minimising the root mean square (RMS) deviation. At each step of the non-linear iteration, D_p for each crossing was estimated using equation (3) and the RMS then re-evaluated with the crossing positions (r_k, θ_k). The model normals, and hence Ψ_k, were evaluated using the current set of a_i's. Thus as the iteration proceeds the model parameters are adjusted and the estimates of D_p change. The solver converges such that the estimated dynamic pressures are self-consistent with the fitted model parameters. Figure 1 illustrates the fitting procedure schematically.

For the simplest case a given magnetopause model can be scaled self-similarly such that the model passes through a given magnetopause crossing. In general, functional forms such as the model considered here can have pressure-dependent geometry and such a scaling does not give correct results. In this work, given a magnetopause crossing (r, θ) we use a Newton-Raphson root-finding method to find D_p which satisfies equation (4), given the relations (5).

We will now apply this new technique to a set of magnetopause crossings observed by Voyagers 1 and 2, and Cassini.

3. Data Set

3.1. Magnetopause crossings

The magnetopause crossings used in this study are comprised of identified crossings from Voyager 1 and 2 PLS [*Bridge et al.*, 1981, 1982] and MAG [*Ness et al.*, 1980, 1982] datasets. These data were revisited such that only crossings identified in both datasets were included.

We also use crossings identified in Cassini magnetometer data [*Dougherty et al.*, 2004, 2005]. These crossings were from the first six orbits of Cassini between 28 June 2004 and 28 March 2005 inclusive. We utilize data from both the fluxgate (FGM) and the vector helium (VHM) instruments on Cassini depending on the telemetry mode of the spacecraft and instrument. Typically 1 second averages are used, although lower resolution data are used when necessary.

Since the magnetopause is a complex boundary consisting of multiple internal and external boundary layers and current sheets, we identify a magnetopause crossing by the transition through the magnetopause current layer (MPCL) identified by the strongest field rotation over the crossing. This definition was adopted to provide an objective criterion for the location of the magnetopause due to its broad complex nature. For situations of high magnetic shear, crossings were readily identified by this strong rotation of the magnetic field. For low-shear crossings the MPCL is less clear in the field data. For such crossings the root-mean-square fluctuation of the field magnitude was used to aid identification of the transition and then the position of the MPCL was identified by the largest rotation. In order to avoid biasing our estimates of the field strength just inside of the magnetopause, we selected intervals of field which were outside any apparent boundary layers [*Russell and Elphic*, 1978; *Russell*, 2003] as observed in the magnetometer data.

Figure 2 shows an example of a magnetopause crossing from the outbound leg of the SOI orbit and which illustrates the above points for a moderately high shear crossing. The magnetopause crossing in question occurred at 17:49:50 UTC SCET on day 186 (4 July) 2004. The magnetospheric magnetic field prior to the crossing was prin-

cipally in B_X and B_Y with a small southward field, B_Z. The orientation of B_X and B_Y indicate that the spacecraft was located in the southern magnetic hemisphere, underneath Saturn's magnetospheric current sheet. Approximately 10 minutes before the spacecraft encountered the MPCL, the field fluctuations were enhanced and variable in all three components of the magnetic field. We interpret this as evidence of a boundary layer (either internal or external, probably internal given the magnitude of the field) and as such place our averaging interval outside of this layer. The magnetic field strength remains roughly constant over the crossing. Whilst the change in B_Z at the MPCL is rather rapid, the change in B_X is very slow over approx 3 minutes. the magnetopause. The fields after the crossing are highly variable with strong fluctuations, characteristic of the magnetosheath.

This analysis produced a list of 64 magnetopause crossings. To avoid introducing bias to the fit due to multiple crossings caused by boundary waves, crossings located within $1R_S$ of each other were averaged together. A spatial averaging was chosen over a temporal one [*Slavin et al.*, 1983] to account for different spacecraft velocities between Voyager and Cassini. This procedure reduced the dataset to 26 crossings.

3.2. Removing the Effect of Dipole Tilt

An observationally determined property of the magnetopause is a distortion from axial symmetry when the magnetic dipole is not perpendicular to the incident solar wind flow [*Tsyganenko*, 1998]. When the dipole points anti-sunward, the magnetotail is displaced in the southward ($-Z_{SM}$) direction and presents a non-axisymmetric obstacle to the solar wind. The solar wind momentum flux on this obstacle results in a gradual deflection of the magnetopause so that it becomes parallel to the solar wind flow at large distances downstream. The conservation of magnetic flux between the northern and southern tail lobes requires that the current sheet also undergoes such a distortion. When the dipole points anti-sunward (sunward) the tail magnetopause undergoes a systematic displacement southward (northward). At the Earth this distortion is periodic on both diurnal and orbital periods. In Saturn's magnetosphere the diurnal variation is very small due to the small tilt between the rotation and dipole axes. This kind of distortion can also be readily seen in magnetohydrodynamic (MHD) simulations of Saturn's magnetosphere [*Hansen et al.*, 2005].

The question is how to account for this tilt in our modeling? Following the direction of empirical magnetic field modelers we start with an undeformed magnetopause, i.e., a magnetopause at equinox where the dipole is perpendicular to the solar wind. By introducing a deformation into the equinox magnetopause surface, effected by a distance and tilt angle-dependent rotation, the magnetopause can be deformed such that at large distances the magnetopause becomes parallel to the solar wind flow direction. We use the transformations of *Tsyganenko* [1998] where a point on the undeformed magnetopause (X, Y, Z) is mapped to a deformed location (X^*, Y^*, Z^*) by the rotation:

$$\begin{aligned} X^* &= X\cos\phi^*(r) + Z\sin\phi^*(r) \\ Y^* &= Y \\ Z^* &= -X\sin\phi^*(r) + Z\cos\phi^*(r) \end{aligned} \tag{6}$$

Where the rotation angle, ϕ^* approaches the tilt of the dipole at small distances and tends to zero for large

planetocentric distances:

$$\sin\phi^* = \frac{R_H}{(R_H^3 + r^3)^{1/3}} \sin\phi \tag{7}$$

Where ϕ is the tilt of the dipole with respect to the solar wind direction and is defined as negative when the dipole is pointing in the anti-sunward direction (as during the Cassini epoch). The tilt angle ranges between $\pm 26^\circ$ over one orbit of Saturn about the Sun. The value of R_H is the hinging distance and is the characteristic distance from Saturn in the noon-midnight meridian where the solar wind starts to have a significant effect on the geometry of the magnetosphere. The hinging distance has approximately the same value as the average distance to the magnetopause and for the same reason. The location of the magnetopause is where the magnetic pressure in the magnetosphere balances the dynamic pressure of the solar wind. The hinging occurs when the dynamic pressure of the solar wind is sufficient to distort the magnetospheric magnetic field which occurs when the dynamic pressure becomes similar to the magnetic pressure. Thus the magnetopause distance and the hinging distance are similar in magnitude. We set the hinging distance to $20R_S$ as this is a typical magnetopause distance at Saturn [*Slavin et al.*, 1985].

The beauty of this transformation is that we can construct an axially symmetric magnetopause shape and then deform the surface to represent a magnetopause distorted by a non-equinox dipole tilt, but we can use the inverse transformation to predict the location of a magnetopause crossing under equinox conditions. Given a set of magnetopause crossings we can remove the effect of the tilt, to first order, with this transform, producing a list of magnetopause crossings whose positions correspond to an ideal, axially symmetric magnetopause. Thus the set of 26 averaged magnetopause crossings were subject to the inverse of equation (6) to produce a final crossing list to be fitted to our chosen axially symmetric functional form.

4. Fitting and Discussion

The above methodology was applied to the set of averaged magnetopause crossings and the resulting model curves are presented in figure 3a. Two curves are plotted with the crossings, representing high and low pressure solar wind conditions. The fitted model parameters a_i are presented in table 1. The uncertainties on each parameter were obtained by a Monte Carlo method. The fitting procedure was repeated 200 times but where the points used in the fitting were selected by sampling 20 times with replacement from the set of averaged crossings. The quoted uncertainties represent the 1σ of the distribution formed from the set of 200 a_i coefficients.

At first this fitting was carried out using a fixed value of $R_H = 20R_S$ but the procedure was repeated using various values for R_H between $5R_S$ and $60R_S$. A systematic variation of R_H was attempted in order to find the hinging distance most consistent with the data. However, the hinging distance of $\approx 40R_S$ from this analysis was very different to what was expected. Because the magnetopause is more directly exposed to the solar wind than the current sheet, the hinging distance should be reduced from a value which is approximately at the distance to the nose of the magnetopause. Hence a value of $R_H \sim 2r_0$ is not consistent with these ideas. We interpret this as an inability of the data to accurately resolve the hinging distance. This is to be expected from a dataset of magnetopause crossings which mostly come

from the flank where the hinging effect is relatively weak compared to the magnetotail. A more expanded study should be attempted with more magnetopause crossings from the high latitude tail where the hinging has more influence on the magnetopause shape. Nevertheless, figure 3c shows the result of applying the warping to the fitted model, using a hinging distance of $R_H = 20R_S$, to represent the approximate conditions during Cassini's arrival at Saturn. The southward displacement of the magnetopause in the tail, due to the tilt of the dipole, is quite evident from this plot.

Figure 4 shows the resulting power-law for the model and the averaged magnetopause crossings about that curve. The shaded areas indicate the error bounds as calculated from the uncertainties in table 1. The scatter of points is well within this bound and forms a tight distribution about the model curve.

4.1. Implication for the Global Configuration of the Magnetosphere

In section 1 we described how different distributions of stress lead to different magnetopause geometries and dynamical behaviors, and that because of rapid rotation and internal mass loading at Saturn we might expect properties very different from the terrestrial magnetopause. Given our model, we now investigate the hypothesis that the centrifugal force in Saturn's equatorial plasma sheet has a significant effect on the properties of the magnetopause.

The pressure dependent parameters in our model, a_2 and to a lesser extent a_4, reflect the underlying physics of Saturn's magnetospheric configuration and dynamics. Firstly the power law exponent $\alpha = -1/a_2 = -4.630$ differs from that expected of a vacuum dipole field, $\alpha = -6$, which is purely due to the r^{-3} behavior of a dipole field. The lower value for our model indicates a magnetopause which responds more sensitively to changes in the dynamic pressure, producing a magnetosphere which is intrinsically more compressible compared to the Earth's rather "stiff" dipole field. The compressibility of the magnetosphere is characteristic of the balance of stresses inside the magnetosphere and our value here is consistent with the importance of hot plasma and inertial forces in determining the configuration of the magnetosphere and hence the magnetopause.

Secondly the negative value of a_4 indicates that the magnetopause flares less with increasing dynamic pressure. This is opposite to the terrestrial case where an increase in dynamic pressure increases the rate of dayside reconnection which increases the amount of tail flux. When the terrestrial tail flux increases, the tail flares out. At the outer planets an issue of timescales arises. The addition of tail flux occurs on a much longer timescale at the giant planets compared with the Earth so any other processes which can alter the tail flaring will dominate in the dynamics of the magnetopause. Thus the negative a_4 in our model is principally the result of the lower dayside reconnection rate.

Polar flattening of Saturn's magnetopause should also not be overlooked in relation to the flaring. At higher latitudes the full 3D non-axisymmetric magnetopause is flattened relative to the equatorial cross section because the centrifugal force at low latitudes stretches the magnetic configuration, presenting a disc-like obstacle to the solar wind. However, due to a lack of higher latitude magnetopause crossings this has not been examined in our study. Also the effect of the static pressure varying in proportion to the dynamic pressure has not been investigated. A more detailed study of the magnetopause

and its flaring should include the polar flattening and a more detailed parameterization for the static pressure, so that the role of pressure in determining the flaring can be fully explored. The polar flattening aspect in particular will be best investigated using the orbits of higher inclination late in the Cassini tour.

4.2. Fitting Stability and Bias

There are two systematic issues which could affect the fit of our model. Firstly since we use a non-linear parameter search, initial values for a_i are required. Secondly (3) does not include particle pressure inside the magnetosphere. Observations have indicated that in the high beta plasma sheet the particle pressure is competitive with the magnetic pressure [*Krimigis et al.*, 1983] violating our equation (3). The first is relatively easy to address. We have repeated our fitting systematically varying our initial conditions and found the best fit parameters to be very stable, generally well within our quoted uncertainties.

The second is rather more difficult to answer fully. If the high beta plasma were present at all of the crossings the effect would be to effectively increase the estimates of D_p by a factor ~ 2 hence the effect should be systematic in the coefficients. However, the high beta plasma is concentrated by the centrifugal force into a thin disc approximately $2R_S$ in half-thickness about the equatorial plane. To assess the effect of such a high beta region we have altered equation (3) for crossings occurring within $2R_S$ of the equatorial plane so that the magnetic pressure is doubled for those crossings, attempting to compensate for the neglect of the particle pressure. With this change made, the fitting was repeated. Of particular concern would be the effect on the power-law and the pressure-dependent flaring parameter a_4. The power-law was found to be sensitive to this analysis, producing a modified power-law of $-1/(5.543 \pm 0.6)$ compared to our model value of $-1/(4.630 \pm 0.4)$ which is a significant deviation. The pressure-dependent flaring parameter was consistent with the best-fit value within the uncertainty. The other two parameters a_1 and a_3 controlling the gross shape and size were both perturbed away from their best-fit values by an amount larger than their estimated uncertainties. The RMS of the fit was increased from $1.566R_S$ for the best-fit model to $1.688R_S$. We also note here that these values of the RMS reinforce our choice of a spatial averaging in section 3.1, recall we average crossings occurring within $1R_S$ which is smaller than this quoted RMS position.

This analysis indicates that the effect of trying to compensate for the high beta environment of crossings near the plasma sheet does have a significant effect on the model fit. The modified-fit power-law does reach a value consistent with a vacuum dipole within the uncertainties of the fitting method, however it is noted that the magnetic field data around many of the low-latitude crossings in our database showed no evidence of high beta plasma just inside the magnetopause. This observation means that the analysis is probably over-correcting for a high-beta plasma, certainly in many cases where it is not justified. On this basis we argue that our basic conclusion, that the power law is significantly different from a vacuum dipole $-1/6$, is unchanged. In addition the model retains the property that the flaring of the model decreases with increasing dynamic pressure.

A final problem is related to the lack of an equilibrium magnetopause as mentioned in the introduction. With sufficient observations one would expect that there is a symmetrical relationship between crossings where the

magnetopause passes closer to the planet where the magnetic field is elevated, to ones where the magnetopause is moving further away leading to a situation where the magnetic field is depressed. With a set of 26 averaged crossings this idealized situation should be realized. The spread of magnetopause crossings in space about our model is also indicative of the validity of this equilibrium assumption. Figure 3b shows the magnetopause crossings plotted with the fitted model, where the crossings have been scaled to a common dynamic pressure. Thus this figure shows the spread of crossings about the magnetopause boundary.

4.3. Comparison with Existing Models

In order to compare this new model with existing models we require dynamic pressures so the model response to external conditions can be compared. To analyze the Slavin and MEBS models we essentially reconstruct the power-law, $r_0 \sim D_p^{-1/\alpha}$ using equation (3) and the method in section 2.1. The stand-off distance corresponding to each crossing is required in order to correctly calculate the model normal and hence the flaring angle. The determination of the stand-off distance by self-similar scaling of the Slavin model is straightforward. It is assumed that the position of the focus does not change and so the self-similarity is about the focus. Given a scaling factor, ζ, the stand-off distance is obtained from $r_0 = x_0 + \zeta L/(1+\epsilon)$.

To calculate the stand-off distance for MEBS, equation (1) is manipulated to form a merit function by considering g and h to be functions of both x and r_0. Given an observed MP crossing, (x, y, z), a value of r_0 can be chosen which satisfies (1). For each crossing r_0 is found by non-linearly minimising (8) using the Downhill-Simplex algorithm [*Press et al.*, 1992]. The coefficients of g and h are tabulated for different values of r_0 in table 1 of *Maurice et al.* [1996] – coefficients for non-tabulated values of r_0 were obtained by linear interpolation.

$$\chi^2(x, y, z, r_0) = \left[\frac{y^2}{h(x, r_0)} + \frac{z^2}{g(x, r_0)} - 1 \right]^2 \qquad (8)$$

Figure 5 shows the results of this analysis. The abscissa on these plots is the X_{KSM} axis. Due to axial symmetry of our new model and the Slavin model, the ordinate axes are the cylindrical distance from the Saturn-Sun line. Because the MEBS model isn't axially symmetric we have chosen to plot that model in an equatorial projection and it should be noted that the difference in location between the observed crossings and their respective curves is mainly an effect of this projection.

Using the 26 averaged magnetopause crossings, for each of the three models we plot the crossings colored according to dynamic pressure, as inferred by our method. We also plot a variety of curves form each model, corresponding to different dynamic pressures, again colored by D_p. For the Slavin model curves, we obtain the pressure from their 1/6.1 power-law scaling, and for our model we use the power-law from our fit which is presented in figure 4. For the MEBS model no such scaling was derived by the authors. To produce the centre panel in figure 5 we use least squares to fit a power-law through the (D_p, r_0) points, as derived above. This power-law is used to color the model curves. The power-law we derive for the MEBS model is $r_0 = (14.9 \pm 0.8) D_p^{-1/7.91 \pm 2}$ which represents a terrestrial scaling within the uncertainties of the fit. It is interesting to note that repeating this analysis for our new model, we obtain a power-law which is

identical within the uncertainty of the fit, to the one derived by our fitting routine. If we repeat the analysis for the Slavin model we obtain a very strange power-law of $r_0 = (5.23 \pm 1)D_p^{-1/3.36\pm0.9}$, quite clearly different from that derived by Slavin.

For a model whose geometry is an accurate representation of the true geometry, the color of the magnetopause crossings should be similar to the color of a nearby model curve. This is equivalent to saying that the point should lie near the power-law curve in $D_p - r_0$ space. Furthermore the magnetopause crossings should "fit" within the range of curves plotted. It is clear from this figure that the three models have very different geometries, although MEBS has a geometry more similar to our new model. The Slavin model flares asymptotically and never achieves a constant tail radius. To match some of the flank crossings this model must be unrealistically scaled in that the stand-off distance at the stagnation streamline is never observed. The mismatch between the observed pressures and the model curves at the flank is quite clear in this model. It should be pointed out however, that this model is principally a model of the dayside magnetopause and so it is unfair to strictly criticize the model in this regard. The MEBS model presents considerably more disorder in it's organisation of the pressures, in comparison to the Slavin model and our new model - it does not have the systematic deviation present between the nose and flanks in the Slavin model.

We can also carry out a visual comparison of our model with recent MHD modeling [*Hansen et al.*, 2005] and theoretical considerations [*Hendricks et al.*, 2005]. Since the model by *Hendricks et al.* [2005] is based on the MEBS model it is unsurprising that their model differs geometrically from ours in a similar way to the MEBS model, even though they refit the rather cumbersome cartesian forms used by *Maurice et al.* [1996] using the *Shue et al.* [1997] functional form. Comparing our model shape with the magnetopause boundary identified in the MHD model of *Hansen et al.* [2005] reveals a close correspondence between our empirical model and their simulation result. Their power law lies slightly outside out best-fit value and error bar. We note with interest that the power-law of *Hansen et al.* [2005] lies almost exactly between our best-fit and high-beta modified fit power-laws from our model.

4.4. Effect on the Bow Shock

The shape of the magnetopause is decisive in determining the location of the bow shock - the more streamlined (blunt) an obstacle, the closer (further) the shock stands in order to deflect the flow. Using empirical relations for the shock distance in terms of the obstacle shape, we can calculate the effect of our new magnetopause model on the shock position. *Farris and Russell* [1994] give the standoff distance of the bow shock D_{BS} in terms of the radius of curvature of the magnetopause, R_C, and the distance to the magnetopause, r_0, as a function of the upstream Mach number M_S and the ratio of specific heats γ.

$$D_{BS} = R_C \left[\frac{r_0}{R_C} + 0.8 \frac{(\gamma - 1)M_S^2 + 2}{(\gamma + 1)(M_S^2 - 1)} \right] \tag{9}$$

The radius of curvature for the *Shue et al.* [1997] model can be shown to be equal to:

$$R_C = \frac{1}{|\kappa|} = \frac{\left(1 + x^2\right)^{3/2}}{|1 - x + 2x^2|} \tag{10}$$

Where $x = K \sin\theta/(1+\cos\theta)$ which is a function of the

angle θ about the surface and of course is also a function of the solar wind dynamic pressure, through the exponent, K. At the stagnation streamline the radius of curvature reduces to $R_C = r_0 = a_1 D_p^{-a_2}$. Towards the terminator the radius of curvature increases because of the flaring of the shape and the two- and three-dimensional shape of the shock should take this into account. For our 1-D purposes along the stagnation streamline we take $R_C = r_0$, thus the standoff distance of the shock is given by:

$$D_{BS} = r_0 \left[1 + 0.8 \frac{(\gamma - 1)M_S^2 + 2}{(\gamma + 1)(M_S^2 - 1)} \right] \qquad (11)$$

Assuming the Alfvén speed is much larger than the sound speed in the solar wind we can equate the solar wind magnetosonic Mach number with the sonic Mach number, and write $M_S^2 = D_p/(\gamma P_0)$ where P_0 is again the static pressure of the solar wind and where we let $\gamma = 5/3$. Equation (11) can be formulated purely in terms of the dynamic pressure. An important quantity in examining the location of the bow shock is the shock-to-magnetopause stand-off ratio which is given in our terms by D_{BS}/r_0. Figure 6 shows a plot of this quantity as a function of dynamic pressure. We can see from this plot that as D_p increases the shock more closely approaches the magnetopause, which is consistent with the observation of increased magnetopause flaring (a blunter obstacle) for lower dynamic pressures.

The terrestrial shock-to-magnetopause ratio lies in the range of $1.3 - 1.4$ hence from figure 6 we can see that a similar situation is realized at Saturn during intervals of very low dynamic pressure, indicating a more blunt magnetopause during these times. From studies of the jovian magnetopause and bow shock [*Huddleston et al.*, 1998] the shock-to-magnetopause ratio is lower, closer to 1.2 indicating a more streamlined obstacle that the shock may approach more closely. Hence our results indicate a behavior of Saturn's bow shock which has more in common with Jupiter that the Earth.

5. Conclusion

We have demonstrated a new technique for obtaining solar wind dynamic pressure estimates from magnetopause crossings, given a model of the magnetopause, in the absence of upstream pressure estimates. This technique has been applied to iteratively fit a magnetopause model which is pressure-dependent. The model has a geometry significantly different to the previous models of Saturn's magnetopause. It was found that the size of the magnetopause varied with a power law significantly different to that of a vacuum dipole indicating that internal plasma pressure was affecting the magnetopause. This is also different to that found by empirical Pioneer/Voyager studies of Saturn's magnetopause [*Slavin et al.*, 1983, 1985] but agrees with recent modeling work by *Hansen et al.* [2005] who found a power-law of $-1/5.2$ for the magnetopause - our model geometry is also similar to their results. We also observed that the flaring of the magnetopause decreased with increasing dynamic pressure which is interpreted as the effect of the stress distribution in Saturn's magnetosphere. In the terrestrial magnetosphere the situation is reversed where the rate of dayside reconnection increases with increasing dynamic pressure which increases the flaring of the tail. We have shown that the model has significantly improved behavior compared to the *Slavin et al.* [1985] and *Maurice et al.* [1996] models. The model geometry we present in this paper is qualitatively consistent with minimum

variance normals indicating that the magnetopause geometry is significantly different from that of the Slavin model (H.J. McAndrews, private communication). Our results are consistent with the hypothesis that the centrifugal force in Saturn's magnetosphere has a significant impact on the morphology and dynamics of the kronian magnetosphere. Magnetometer observations indicate the presence of a thin current sheet and stretched disc-like field morphology consistent with this hypothesis. The magnetopause results we have presented are the global consequences of such a configuration.

It is interesting to look at the predictions made by the model and by our method of inferring the pressure in situations where we understood magnetospheric dynamics to have occurred. During the SOI pass of Cassini, a compression event was suspected while Cassini was inside the magnetosphere [*Dougherty et al.*, 2005] and signatures of this event were detected in fields and particles instruments [*Bunce et al.*, 2005]. Our model shows that the stand-off distance at SOI inbound was $25.5R_S$ which changed to $18.3R_S$ when the spacecraft re-encountered the magnetopause outbound. Examining the inferred pressures we see clearly that the pressure increased by more than a factor of 3 while Cassini was inside the magnetosphere, from $0.0220nPa$ inbound to $0.0756nPa$ outbound. Similar analyses can be done on other interesting periods. During the Voyager 1 encounter with Saturn there was a similar compression to SOI and during Voyager 2 the magnetopause expanded considerably. Comparisons such as these highlight the variability in the location of the kronian magnetopause. A study of this variability is underway and will be the subject of a future paper.

The effect of internal plasma pressure on the pressure balance requires further attention. The limited attempt to account for this by doubling the internal pressure for all crossings near the equatorial plane should be replaced with real measurements of the internal plasma pressure and a suitable modification of (3). A comparison of our model dynamic pressure estimates with actual measurements of the dynamic pressure would also aid to establish the validity of the method. An expanded study taking into account dawn-dusk asymmetry and polar flattening will be carried out when an expanded list of magnetopause crossings is available with a wider local-time and latitudinal coverage.

It has been suggested [*Espinosa et al.*, 2003; *Southwood and Kivelson*, 2005] that the internal pressure in Saturn's magnetosphere varies with Saturn longitude and that this affects the location of the magnetopause. In steady solar wind conditions, an observer located near the magnetopause would cross the magnetopause twice per rotation period. We have not made an attempt to incorporate this effect into our model. A principal reason for neglecting this effect is that the rotation rate of Saturn is not well known so any attempt to use the existing longitude definition will introduce uncertainties because of longitudinal smearing. A more thorough investigation of this effect should be carried out when a more robust definition of longitude is available.

Finally the power of the general deformation [*Tsyganenko*, 1998] technique in generating asymmetric magnetopause shapes should not be overlooked. The technique is flexible enough to not only model tilt-related deformation, but also dawn-dusk asymmetries and polar flattening without the use of cumbersome cartesian forms.

Acknowledgments. The authors would like to thank S. Joy, K.C. Hansen, M.G. Kivelson, H.J. McAndrews, S.E. Milan, D.J. Southwood and R.J. Walker for useful comments and

discussions. CSA carried out part of this work during a stay at the Institute of Geophysics and Planetary Physics, UCLA, and CSA would like to acknowledge the kindness and hospitality of the staff and students during his stay there. CSA was supported in this work by a PPARC Quota Studentship, CB and NA by PPARC, MKD by a PPARC Senior Fellowship, and KKK was supported by NASA.

References

Blanc, M., et al. (2002), Magnetospheric and plasma science with Cassini-Huygens, *Space Sci. Rev.*, *104*, 254–346.

Bridge, H., et al. (1981), Plasma observations near Saturn: Initial results from Voyager 1, *Science*, *212*(4491), 217–224.

Bridge, H., et al. (1982), Plasma observations near Saturn: Initial results from Voyager 2, *Science*, *215*(4532), 563–570.

Bunce, E., S. Cowley, D. Wright, A. Coates, M. Dougherty, N. Krupp, W. Kurth, and A. Rymer (2005), In situ observations of a solar wind compression-induced hot plasma injection in Saturn's tail, *Geophys. Res. Lett.*, *32*, L20S04.

Crary, F., et al. (2005), Solar wind dynamic pressure and electric field as the main factors controlling saturn's aurorae, *Nature*, *433*, 720–722.

Dougherty, M., et al. (2004), The Cassini Magnetic Field Investigation, *Space Sci. Rev.*, *114*, 331–383.

Dougherty, M., et al. (2005), Cassini Magnetometer Observations During Saturn Orbit Insertion, *Science*, *307*, 1266–1270.

Espinosa, S., D. Southwood, and M. Dougherty (2003), How can Saturn impose its rotation period in a noncorotating magnetosphere?, *J. Geophys. Res.*, *108*(A2), 1086, doi:10.1029/2001JA005084.

Farris, M., and C. Russell (1994), Determining the standoff distance of the bow shock: Mach number dependence and use of models, *J. Geophys. Res.*, *99*(A9), 17,681–17,689.

Hansen, K., A. Ridley, G. Hospodarsky, N. Achilleos, M. Dougherty, T. Gombosi, and G. Tóth (2005), Global MHD Simulations of Saturn's Magnetosphere at the Time of Cassini Approach, *Geophys. Res. Lett.*, *32*, L20S06, doi:10.1029/2005GL022835.

Hendricks, S., F. Neubauer, M. Dougherty, N. Achilleos, and C. Russell (2005), Variability in Saturn's Bow Shock and Magnetopause from Pioneer and Voyager: Probabilistic Predictions and Initial Observations by Cassini, *Geophys. Res. Lett.*, *32*, L20S08, doi:10.1029/2005GL022569.

Huddleston, D., C. Russell, M. Kivelson, K. Khurana, and L. Bennett (1998), Location and shape of the jovian magnetopause and bow shock, *J. Geophys. Res.*, *103*(E9), 20,075–20,082.

Joy, S., M. Kivelson, R. Walker, K. Khurana, C. Russell, and T. Ogino (2002), Probabilistic models of the Jovian magnetopause and bow shock locations, *J. Geophys. Res.*, *107*(A10), 1309, doi:10.1029/2001JA009146.

Kawano, H., S. Petrinec, C. Russell, and T. Higuchi (1999), Magnetopause shape determinations from measured position and estimated flaring angle, *J. Geophys. Res.*, *104*(A1), 247–261.

Krimigis, S., J. Carbary, E. Keath, T. Armstrong, L. Lanzerotti, and G. Gloeckler (1983), General characteristics of hot plasma and energetic particles in the Saturnian magnetosphere - Results from the Voyager spacecraft, *J. Geophys. Res.*, *88*, 8871–8892.

Macek, W., W. Kurth, R. Lepping, and D. Sibeck (1992), Distant magnetotails of the outer magnetic planets, *Adv. Space. Res.*, *12*(8), 47–55.

Maurice, S., I. Engle, M. Blanc, and M. Skubis (1996), Geometry of Saturn's magnetopause model, *J. Geophys. Res.*, *101*(A12), 27,053–27,059.

Mead, G., and D. Beard (1964), Shape of the geomagnetic field solar wind boundary, *J. Geophys. Res.*, *69*, 1169.

Ness, N., M. Acuña, R. Lepping, J. Connerney, K. Behannon, L. Burlaga, and F. Neubauer (1980), Magnetic field studies by Voyager 1: Preliminary results at Saturn, *Science*, *207*(4491), 211–217.

Ness, N., M. Acuña, K. Behannon, L. Burlaga, J. Connerney, R. Lepping, and F. Neubauer (1982), Magnetic field studies by Voyager 2: Preliminary results at Saturn, *Science*, *215*(4532), 558–563.

Petrinec, S., and C. Russell (1997), Hydrodynamic and MHD equations across the bow shock and along the surfaces of planetary obstacles, *Space Sci. Rev.*

Press, W., S. Teukolsky, W. Vetterling, and B. Flannery (1992), *Numerical Recipes in C: The Art of Scientific Computing*, 2nd ed., Cambridge University Press.

Russell, C. (2003), The structure of the magnetopause, *Planet. Space Sci.*, *51*, 731–744.

Russell, C., and R. Elphic (1978), Initial ISEE magnetometer results: Magnetopause observations, *Space Sci. Rev.*, *22*, 681–715.

Shue, J.-H., and P. Song (2002), The location and shape of the magnetopause, *Planet. Space Sci.*, *50*, 549–558.

Shue, J.-H., J. Chao, H. Fu, C. Russell, P. Song, K. Khurana, and H. Singer (1997), A new functional form to study the solar wind control of the magnetopause size and shape, *J. Geophys. Res.*, *102*(A5), 9497–9511.

Shue, J.-H., C. Russell, and P. Song (2000), Shape of the low-latitude magnetopause: comparison of models, *Adv. Space. Res.*, *25*(7/8), 1471–1484.

Slavin, J., and R. Holzer (1981), Solar Wind Flow About the Terrestrial Planets 1. Modeling Bow Shock Position and Shape, *J. Geophys. Res.*, *86*(A13), 11,401–11,418.

Slavin, J., E. Smith, P. Gazis, and J. Mihalov (1983), A Pioneer-Voyager study of the solar wind interaction with Saturn, *Geophys. Res. Lett.*, *10*(1), 9–12.

Slavin, J., E. Smith, J. Spreiter, and S. Stahara (1985), Solar wind flow about the outer planets: Gas dynamic modeling of the Jupiter and Saturn bow shocks, *J. Geophys. Res.*, *90*(A7), 6275–6286.

Sonnerup, B. O., and L. Cahill (1967), Magnetopause Structure and Attitude from Explorer 12 Observations, *J. Geophys. Res.*, *72*(1), 171–183.

Southwood, D., and M. Kivelson (2005), Saturnian magnetospheric dynamics, in *Eos Trans. AGU, 86(52), Fall. Meet. Suppl., Abstract P51E-04*.

Spreiter, J., and A. Alksne (1970), Solar-wind flow past objects in the solar system, *Ann. Rev. Fluid Mech.*, *2*, 313–354.

Stahara, S., R. Rachiele, J. Spreiter, and J. Slavin (1989), A Three dimensional gasdynamic model for solar wind flow past nonaxisymmetric magnetospheres: Application to Jupiter and Saturn, *J. Geophys. Res.*, *94*(A10), 15,353–13,365.

Tsyganenko, N. (1998), Modeling of twisted/warped magnetospheric configurations using the general deformation method, *J. Geophys. Res.*, *103*(A10), 23,551–23,563.

C. S. Arridge, Space and Atmospheric Physics, The Blackett Laboratory, Imperial College London, Prince Consort Road, South Kensington, London, SW7 2BW, UK. (christopher.arridge@imperial.ac.uk)

Appendix A: Application of the Model

The model developed in this paper can be applied to many different scientific problems where knowledge of the magnetopause stand-off distance, an estimate of the solar wind dynamic pressure, or an understanding of the local magnetopause geometry are invaluable. Furthermore such models are useful in science planning and visualization, and in the development of other models such as global magnetospheric magnetic field models and bow shock models.

To aid the use of this model we illustrate several uses of our model in addressing some of the issues above. In addition, computer programs implementing our model which provides model normals, estimated pressures, and extrapolated stand-off distances are available from the authors for use with Matlab, IDL, ANSI C, and Fortran.

A1. Plotting Model Boundaries

Solve equation (4) for various values of θ over a suitable interval such as $\pm\pi/2$ where a suitable dynamic pressure is selected and substituted into (5). To obtain a magnetopause which is deformed for a given dipole tilt, take the pairs of (r, θ) convert to cartesian coordinates (in solar magnetospheric coordinates) and then apply the transformation (6). Performing the substitutions yields:

$$\begin{aligned} X^* &= r\cos\theta\cos\Psi^*(r) + r\sin\theta\sin\Psi^*(r) \\ Z^* &= -r\cos\theta\Psi^*(r) + r\sin\theta\cos\Psi^*(r) \end{aligned} \tag{A1}$$

The tilt angle Ψ^* should be calculated for each point using (7) where Saturn's tilt angle can be computed using NAIF SPICE software, for example. Note that to obtain a 3D magnetopause shape this needs to be done for a range of angles, $0 \leq \phi < \pi/2$, about the symmetry axis which introduces a Y component.

A2. Calculation of Stand-Off Distances

To calculate the stand-off distance corresponding to a given magnetopause crossing the model D_p, through equations (5), must be adjusted such that the model passes through the observed point. For this work, this has been achieved using a root-finding method based on Newton-Raphson iteration. Given an initial estimate for the dynamic pressure, D_p^n, where the superscript indicates an iteration, the next iteration for the dynamic pressure is given by:

$$D_p^{n+1} = D_p^n + \frac{r - r(\theta, D_p^n)}{a_4 r X - \frac{a_2 r}{D_p^n}} \tag{A2}$$

Where $X = \log(2/(1+x/r))$ and x is the location of the observed magnetopause crossing in solar magnetospheric coordinates and r is the planetocentric distance to the observed crossing. This equation can then be iterated until D_p is accurate to within some tolerance set by the demands of the application. In this work a fractional change of smaller than 1% is required for the root-finder to terminate. Given D_p from this method, the stand-off distance is then simply found from (5a).

A3. Calculation of Model Normals

Knowing D_p for a given magnetopause crossing we can find the normal to the model at the point of the crossing (or any point on the surface). We write a position on the magnetopause as (r, θ, ϕ) which are related to cartesian KSM coordinates by $\theta = cos^{-1}x/r$ and $\phi = tan^{-1}z/y$. The normal vector can be found from:

$$\mathbf{n} = \frac{\partial \mathbf{r}}{\partial \theta} \times \frac{\partial \mathbf{r}}{\partial \phi}; \tag{A3}$$

Where,

$$\frac{\partial \mathbf{r}}{\partial \theta}|_x = r\sin\theta\left(\frac{K\cos\theta}{1+\cos\theta} - 1\right) \tag{A4a}$$

$$\frac{\partial \mathbf{r}}{\partial \theta}|_y = r\cos\phi\left(\cos\theta + \frac{K\sin^2\theta}{1+\cos\theta}\right) \tag{A4b}$$

$$\frac{\partial \mathbf{r}}{\partial \theta}|_z = r\sin\phi\left(\cos\theta + \frac{K\sin^2\theta}{1+\cos\theta}\right) \tag{A4c}$$

$$\frac{\partial \mathbf{r}}{\partial \phi} = r\sin\theta\,(0, -\sin\phi, \cos\phi) \tag{A5}$$

The normal in the noon-midnight meridional plane can

easily be found from the inner product of (A3) and the solar wind direction - nominally in the direction of x so it is sufficient to take the x component of (A3). Knowing the normal, an estimation of the pressure assuming a pressure balance can be found using (3) with a measurement of the magnetospheric magnetic pressure.

Table 1. Fitted coefficients, uncertainties, and model RMS for our model.

a_1	10.36 ± 0.9
a_2	0.2160 ± 0.02
a_3	0.7680 ± 0.02
a_4	-1.385 ± 0.2
α	4.630 ± 0.4
RMS	$1.566 R_S$

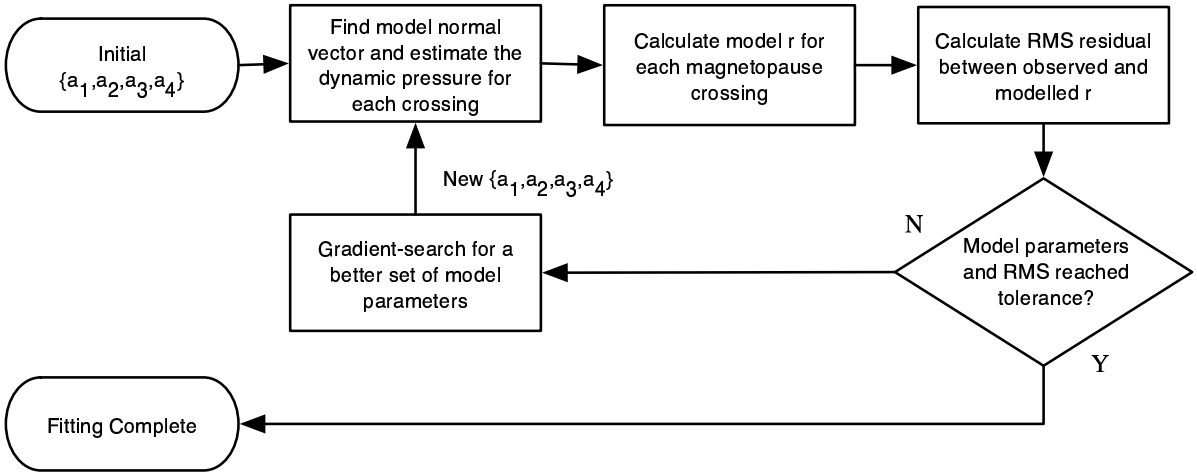

Figure 1. Flow-chart showing the method for fitting the observed magnetopause crossings to the pressure-dependent functional form described by equations (4,5).

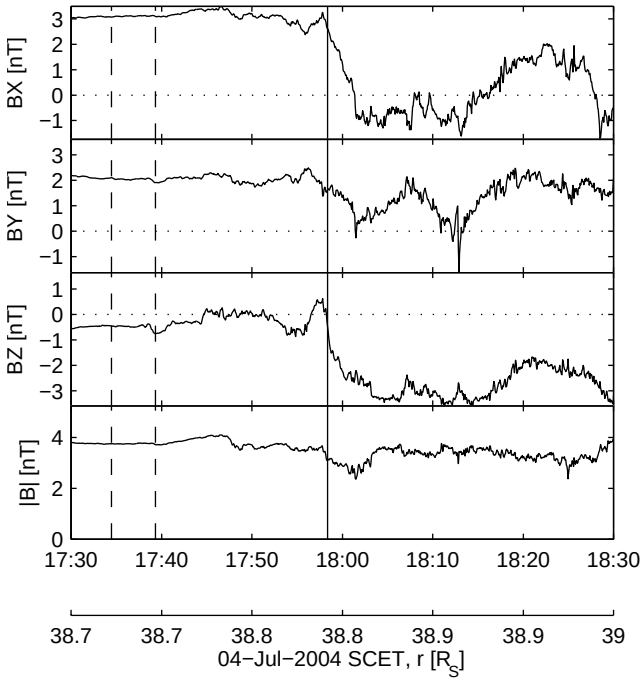

Figure 2. Example magnetopause crossing on 4 July 2004 during the outbound portion of Cassini's Saturn Orbit Insertion (SOI) revolution. The three components of the field in KSM coordinates are in the top three panels with the field magnitude in the fourth. The solid vertical line indicates the magnetopause current layer and the two dashed lines delimit the interval used to estimate the magnetic pressure just inside the magnetopause. The interval is chosen so it avoids obvious boundary layers or other magnetic structures evident in the data. These data are from the VHM instrument on Cassini.

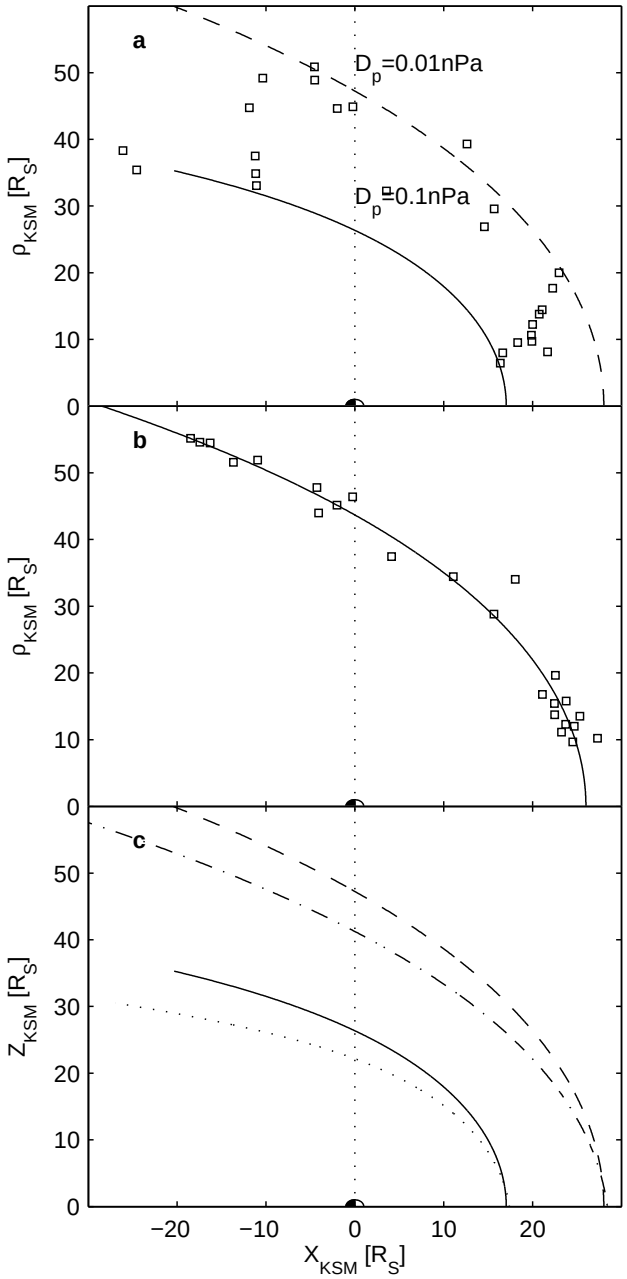

Figure 3. The geometry of the new model. Panel (a) shows the crossings used for the fitting plotted with the model at two different dynamic pressures: the dashed line is for $D_p = 0.01nPa$ and the solid line $D_p = 0.1nPa$. The lack of self-similarity is obvious from the two curves plotted here. (b) Shows the crossings used in our fitting collapsed onto a common dynamic pressure surface (selected so that the magnetopause standoff distance is $26R_S$. The magnetopause crossings were scaled assuming that the change in position angle of each magnetopause crossing is small compared to the change in radial position. It can be shown that this is valid for the range of angles and pressures in our dataset. c) Presents the model for two different dynamic pressures where the effect of dipole tilt has been taken into account using equation (A1). These have been plotted for the dipole tilt at the Cassini SOI epoch ($\approx -25°$). The two pressures are $D_p = 0.01nPa$ (– and -.) and $D_p = 0.1nPa$ (- and ..). The southward displacement of the warped curves (.. and -.) from unwarped (equinox) curves (- and –) in the tail magnetopause is clearly seen in this figure. In each of these plots the coordinates are along the X_{KSM} axis and in the direction perpendicular to this, $\rho_{KSM} = (Y_{KSM}^2 + Z_{KSM}^2)^{1/2}$, except for panel (c) where the Z_{KSM} axis is used.

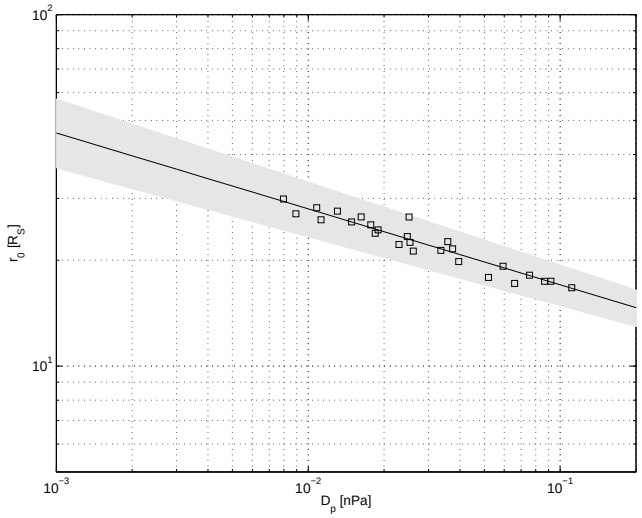

Figure 4. The power-law relationship between stand-off distance and dynamic pressure for the model presented here. The shaded region indicates the uncertainty in this power-law, as derived from the uncertainties in table 1. All of these points fit well within this region and have a tight distribution about the best-fit curve.

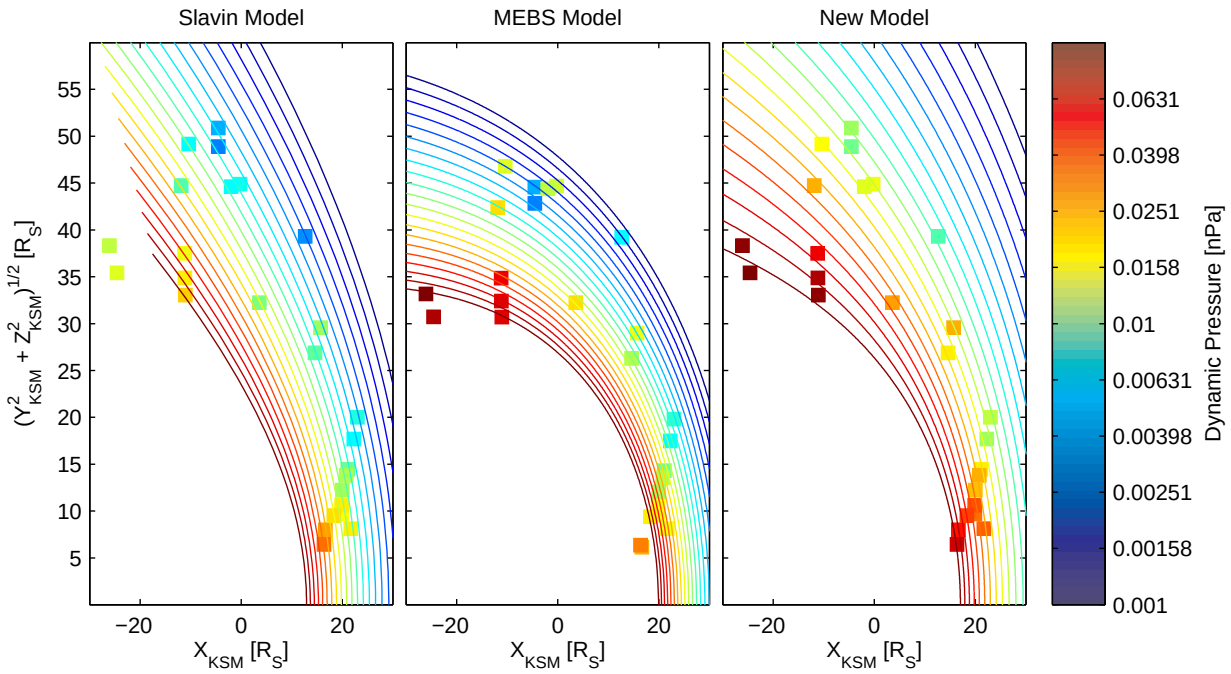

Figure 5. Comparison of the new model presented in this paper, with a corresponding analysis carried out for the Slavin and MEBS models. In each plot the method described in section 2.1 has been applied to infer the dynamic pressure of each magnetopause crossing which have been plotted and colored according to the inferred pressure. A number of curves from each model are also plotted and colored according to the pressure-parameterization of that model. Since the MEBS model was developed with no such parametersiation we have fitted a power-law to the results of our analysis to provide such a power-law. For each model, the color of each magnetopause crossing should lie close to where a similar-colored model curve lies. For an accurate model there should be a smooth graduation in color between the high pressure crossings close to the planet and the low pressure crossing farther away, and the model curves should largely contain the observed crossings. As can be seen, the Slavin and MEBS models are fairly disordered in this regard, whereas our new model largely exhibits a smooth change in pressure indicating that our model is more accurately representing Saturn's magnetopause geometry. Since the MEBS model is not axially symmetric, in that panel the ordinate axis corresponds to the $|Y|$ axis of the MEBS model.

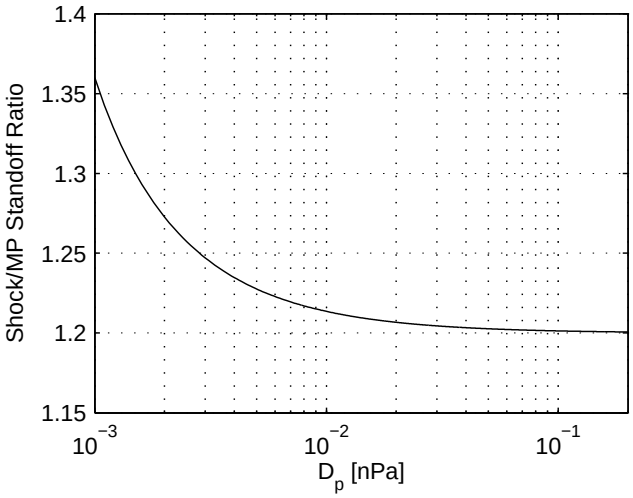

Figure 6. Plot showing the ratio between the shock and magnetopause stand-off distances as a function of solar wind dynamic pressure. Equivalently this curve can be considered as the planetocentric distance to the bow shock, in units of the distance to the magnetopause along the stagnation streamline. The figure shows that the shock more closely approaches the magnetopause under conditions of higher dynamic pressure which is a consequence of the more streamlined magnetopause shape at higher pressures.